Multifrequency control pulses for multilevel superconducting quantum circuits

Anne M. Forney
Gettysburg College, Gettysburg, Pennsylvania 17325, USA

Steven R. Jackson and Frederick W. Strauch*
Williams College, Williamstown, Massachusetts 01267, USA

(Received 5 October 2009; published 8 January 2010)

Superconducting quantum circuits, such as the superconducting phase qubit, have multiple quantum states that can interfere with ideal qubit operation. The use of multiple frequency control pulses, resonant with the energy differences of the multistate system, is theoretically explored. An analytical method to design such control pulses is developed, using a generalization of the Floquet method to multiple frequency controls. This method is applicable to optimizing the control of both superconducting qubits and qudits and is found to be in excellent agreement with time-dependent numerical simulations.

DOI: 10.1103/PhysRevA.81.012306 PACS number(s): 03.67.Lx, 03.65.Pm, 05.40.Fb

I. INTRODUCTION

Superconducting circuits are a promising approach to building a large-scale quantum information processor. Over the past ten years quantum coherence times have improved by 2 orders of magnitude, from nanosecond to microsecond time scales [1–6]. With this improvement has come increased attention to the fundamental quantum processes that arise when these circuits are controlled by microwave fields. A recurring theme in recent experiments was to characterize the multiple quantum levels that can be excited in either the frequency or time domain. On the one hand, these extra levels can interfere with ideal qubit operation. There have been many theoretical studies of the imperfections that arise due to higher energy levels, a phenomenon called "leakage" [7]. On the other hand, these higher levels can also be used advantageously, either to mediate quantum interactions between qubits [8] or to process quantum information with higher dimensional quantum systems called qudits [9]. Recently, multiple levels of a superconducting phase qubit were addressed by multifrequency control fields to emulate a quantum spin (with spin $> 1/2$) [10]. From either perspective, it is an important task to develop theoretical tools to model these quantum processes simply and accurately.

Most theoretical work focused on the deviations from ideal qubit behavior during Rabi oscillations and how these can be mitigated by pulse shaping techniques [11,12]. Optimal control theory was also applied to this problem [13–15] and recent work has indicated that arbitrarily fast control is possible using certain choices of pulses [16]. The presence of higher levels is also problematic for coupled-qubit operation. These arose in the study of coupled phase qubits: The spectroscopic signatures were analyzed in Ref. [17] while a nonadiabatic controlled-phase gate using the higher levels was first proposed in Ref. [8].

Experimentally, the effect of the higher levels in a superconducting circuit was demonstrated in transmon circuits [18] both in single-qubit operations [19] and recently in a two-qubit controlled-phase gate [20], similar to the phase-qubit gate described previously. For phase qubits, multilevel Rabi oscillations [21,22] and multiphoton Rabi oscillations [23] were analyzed in some detail while a sensitive characterization of leakage was demonstrated by a Ramsey filter method [24]. Recently, interference effects due to multiple frequency controls were demonstrated [25], thus realizing effects related analogous to electromagnetically induced transparency [26,27].

In this article we develop a simple theoretical framework to describe the control of multiple levels in a superconducting phase qubit using multifrequency control fields. We start from an early proposal to reduce leakage during qubit manipulation by resonantly canceling off-resonant transitions to the higher energy levels [28]. Numerical simulations are used to demonstrate that this approach can optimize a quantum transition on the multilevel qubit. These results are explained using the many-mode generalization [29] of the Floquet formalism [30] for a Hamiltonian that is periodic in time. We show that multifrequency control fields can produce a unique quantum interference to optimize the desired transition, without complex pulse shaping. We further show how the Floquet formalism can describe other interference effects when driving multiple transitions.

This article is organized as follows. In Sec. II we describe the basic model of a phase qubit. In Sec. III we introduce the Floquet formalism for a single frequency control pulse, reproducing the effects that occur in three-level Rabi oscillations. This formalism generalizes the rotating-wave approximation, taking a time-dependent problem to a time-independent problem (with a much larger state space). In Sec. IV we extend the Floquet formalism to include control fields with multiple frequencies. This analytical approach is used to optimize a transition between the first two levels of the phase qubit. These ideas are confirmed in Sec. V through numerical optimizations of square and Gaussian control pulses. We return to the Floquet formalism in Sec. VI to predict beating effects relevant to the recent spin-emulation experiment [10]. Finally, we conclude our study in Sec. VII, while certain theoretical results are detailed in the Appendix.

II. PHASE-QUBIT HAMILTONIAN

The phase qubit is generally based on a variation of the current-biased Josephson junction [1]. This is described by

*Frederick.W.Strauch@williams.edu

the following Hamiltonian

$$H = 4E_c\hbar^{-2}p_\gamma^2 - E_J\left[\cos\gamma + (I/I_c)\gamma\right]. \tag{1}$$

The dynamical variables are γ, the gauge-invariant phase difference, and p_γ its conjugate momentum subject to the commutation relation $[\gamma, p_\gamma] = i\hbar$. The other parameters are the junction's bias and critical currents $I = I_{dc}$ and I_c, the capacitance C, and the energy scales $E_J = \hbar I_c/2e$ and $E_c = e^2/2C$.

To describe Rabi oscillations, we will let the bias current be time dependent, of the form $I = I_{dc} - I_{ac}(t)$, and restrict the Hamiltonian to the lowest four energy levels to find

$$H = H_0 + f(t)X, \tag{2}$$

where we divide the Hamiltonian into its unperturbed, time-independent form

$$H_0 = \begin{pmatrix} E_0 & 0 & 0 & 0 \\ 0 & E_1 & 0 & 0 \\ 0 & 0 & E_2 & 0 \\ 0 & 0 & 0 & E_3 \end{pmatrix}, \tag{3}$$

and a set of dimensionless matrix elements

$$X = \begin{pmatrix} x_{00} & x_{01} & x_{02} & x_{03} \\ x_{01} & x_{11} & x_{12} & x_{13} \\ x_{02} & x_{12} & x_{22} & x_{23} \\ x_{03} & x_{13} & x_{23} & x_{33} \end{pmatrix}. \tag{4}$$

The energy levels E_n and the matrix elements x_{nm} can be calculated by either diagonalizing the washboard potential directly or by some approximation scheme. The latter can be efficiently performed by first approximating the washboard potential as a cubic oscillator of the form

$$H = \hbar\omega_0\left(\tfrac{1}{2}p^2 + \tfrac{1}{2}x^2 - \lambda x^3\right), \tag{5}$$

where $\hbar\omega_0 = \sqrt{8E_cE_J}[1 - (I_{dc}/I_c)^2]^{1/4}$ and $\lambda = 1/\sqrt{54N_s}$ with N_s given by

$$N_s = \frac{\Delta U}{\hbar\omega_0} \approx \frac{2^{3/4}}{3}\left(\frac{E_J}{E_c}\right)^{1/2}\left(1 - \frac{I_{dc}}{I_c}\right)^{5/4}. \tag{6}$$

The resulting energies and matrix elements, calculated using perturbation theory, are found in the Appendix. Finally, the driving field has the explicit form

$$f(t) = \frac{I_{ac}(t)}{I_c}E_J\left(\frac{8E_c}{\hbar\omega_0}\right)^{1/2} \approx -\hbar\frac{d\omega_0}{dI}\frac{I_{ac}(t)}{3\lambda}. \tag{7}$$

III. SINGLE-MODE FLOQUET THEORY: THREE-LEVEL RABI OSCILLATIONS

For Rabi oscillations in the presence of strong driving there are deviations from two-level behavior that can be analyzed using a three-level model. Previous studies [11,12,31,32] using the rotating-wave approximation identified three main features. First, the coherent oscillations between the ground and first excited state are accompanied by oscillations to the second excited state. Second, there is a reduction in a Rabi frequency. Finally, there is a Stark shift of the optimal resonance condition. All of these effects have been seen experimentally [23,24,32]. In this section we theoretically derive these effects by introducting the Floquet formalism [30].

First, we let the driving field be given by $f(t) = A\cos\omega t$. Then, we expand the wave function as a Fourier series

$$|\Psi(t)\rangle = \sum_{n=-\infty}^{\infty} |\psi_n(t)\rangle e^{in\omega t}. \tag{8}$$

Finally, substituting this series into the Schrödinger equation $i\hbar d|\Psi\rangle/dt = H|\Psi\rangle$, with $H = H_0 + AX\cos\omega t$, we match terms proportional to $e^{in\omega t}$ on each side. The resulting equations to be solved are

$$i\hbar\frac{d|\psi_n\rangle}{dt} = (H_0 + n\hbar\omega)|\psi_n\rangle + \frac{1}{2}AX(|\psi_{n-1}\rangle + |\psi_{n+1}\rangle). \tag{9}$$

Letting $|\psi_n(t)\rangle = e^{-i\bar{E}t/\hbar}|\psi_n(0)\rangle$, we find that these coupled equations are equivalent to a time-independent Schrödinger equation $\mathcal{H}_F|\Psi\rangle = \bar{E}|\Psi\rangle$ for the infinite state $|\Psi\rangle = \sum_{n=-\infty}^{\infty}|\psi_n\rangle \otimes |n\rangle$ with the Floquet-Hamiltonian matrix

$$(\mathcal{H}_F)_{n,m} = (H_0 + n\hbar\omega)\delta_{n,m} + \tfrac{1}{2}AX(\delta_{n,m-1} + \delta_{n,m+1}). \tag{10}$$

The labels n and m can be interpreted as photon numbers for the driving field and the overall state as that of the combined system and field.

In general, this approach has replaced a finite-dimensional time-dependent problem with an infinite-dimensional time-independent problem. To solve the latter we can approximate the infinite matrix by one of its sub-blocks. For the problem at hand, the lowest-order approximation is to include only three states: $|0,0\rangle$, $|1,-1\rangle$, and $|2,-2\rangle$, where we are using the notation of the form $|s,n\rangle$ to indicate the system in state $s = 0$, 1, and 2 with $n = 0$, -1, and -2 photons, respectively. Negative photon numbers are allowed here as these are differences from the average photon number in a semiclassical state [30]. After removing an overall constant energy E_0, the resulting Floquet matrix takes the form

$$\mathcal{H}_F = \hbar\begin{pmatrix} 0 & \Omega_{01}/2 & 0 \\ \Omega_{01}/2 & \omega_{01} - \omega & \Omega_{12}/2 \\ 0 & \Omega_{12}/2 & \omega_{02} - 2\omega \end{pmatrix}, \tag{11}$$

where $\hbar\Omega_{01} = Ax_{01}$, $\hbar\omega_{01} = E_1 - E_0$, and $\hbar\omega_{02} = E_2 - E_0$. For convenience we also define $\hbar\omega_{12} = E_2 - E_1$; note that $\omega_{02} = \omega_{12} + \omega_{01}$. Note also that this approach reproduces the rotating-wave approximation exactly, while including more states allows for systematic corrections due to strong multiphoton processes such as the Bloch-Siegert shift [30]. The resulting dynamics can be found by diagonalizing the Floquet matrix. For this Hamiltonian exact results are available [12,32]; here we will adopt a perturbative approach.

To simplify the following, we consider the case of near resonance with $\delta = \omega - \omega_{01} \ll \Omega_{01}$ and approximate $\Omega_{12} \approx \sqrt{2}\Omega_{01}$. For weak driving, the largest scale in the problem is $\Delta = 2\omega - \omega_{02} \approx \omega_{01} - \omega_{12} \approx 5\omega_0/(36N_s)$. This corresponds to the anharmonicity of the system being inversely proportional to N_s. For Rabi frequencies near this value three-level effects become important [12,32]. Therefore, to see deviations from two-level behavior we use perturbation theory in the small parameters δ/Ω_{01} and Ω_{01}/Δ, starting from the zeroth-order eigenstates $(|0,0\rangle \pm |1,-1\rangle)/\sqrt{2}$ and $|2,-2\rangle$. Using standard methods of perturbation theory, we compute the (normalized) eigenstates $|v_\ell\rangle$ and eigenvalues $\bar{E}_\ell$,

from which we calculate the time-dependent amplitudes

$$a_s(t) = \sum_{\ell=0}^{2} e^{-i\bar{E}_\ell t/\hbar}\langle s, -s|v_\ell\rangle\langle v_\ell|\psi(0)\rangle, \tag{12}$$

where we assume that $\psi(0)\rangle = |0, 0\rangle$. This calculation is best done using a computer, as the required order of perturbation theory is second order for the wave function and fourth order for the energy. Alternatively, one can expand the exact eigenvalues using the roots of a cubic polynomial. In either case we find that the amplitudes satisfy

$$a_0(t) \approx \cos(\Omega t/2) - i\sin(\Omega t/2)\left(\frac{\delta}{\Omega_{01}} - \frac{\Omega_{01}}{2\Delta}\right), \tag{13}$$

$$a_1(t) \approx -i\sin(\Omega t/2)\left[1 - \frac{\Omega_{01}^2}{4\Delta^2} - \frac{1}{2}\left(\frac{\delta}{\Omega_{01}} - \frac{\Omega_{01}}{2\Delta}\right)^2\right], \tag{14}$$

and

$$a_2(t) \approx -i\frac{\sqrt{2}\Omega_{01}}{2\Delta}\sin(\Omega t/2), \tag{15}$$

where the Rabi frequency Ω is given by

$$\Omega = \Omega_{01}\left(1 - \frac{\Omega_{01}^2}{4\Delta^2}\right) + \frac{\Omega_{01}}{2}\left(\frac{\delta}{\Omega_{01}} - \frac{\Omega_{01}}{2\Delta}\right)^2. \tag{16}$$

There are many things to note about this solution. First, we observe that both $a_1(t)$ and $a_2(t)$ are proportional to $\sin(\Omega t/2)$. Thus, transitions from the ground to the first excited state leak out to the second excited state, with probability

$$p_2(t) = |a_2(t)|^2 \approx \frac{\Omega_{01}^2}{2\Delta^2}\sin^2(\Omega t/2). \tag{17}$$

Avoiding this leakage through pulse shapes was the subject of much investigation [11–13,16]. In addition to this error, however, is the reduction of $p_1(t) = |a_1(t)|^2$ by the factor depending on δ/Ω_{01}. This is due to the fact that, when coupled to the second excited state, the $0 \to 1$ transition is no longer located at $\delta = \omega - \omega_{01} = 0$, but rather at $\delta = \Omega_{01}^2/(2\Delta)$, that is,

$$\omega \approx \omega_{01} + \frac{\Omega_{01}^2}{2(\omega_{01} - \omega_{12})}. \tag{18}$$

This is the effective ac Stark shift measured in experiments [23,32]. As shown in the following, it must be compensated for high-fidelity qubit rotations. Finally, the on-resonance Rabi frequency is given by

$$\Omega_R \approx \Omega_{01}\left(1 - \frac{\Omega_{01}^2}{4(\omega_{01} - \omega_{12})^2}\right). \tag{19}$$

Its reduction is due to the dressed eigenstates of the system and was also measured experimentally [21–23,32].

IV. TWO-MODE FLOQUET THEORY: OPTIMIZED RABI OSCILLATION

In the presence of a control field of the form

$$f(t) = A_1\cos\omega_1 t + A_2\cos(\omega_2 t + \phi), \tag{20}$$

the Floquet method can be generalized [29] to include two sets of photon states for the two oscillatory components of the field. That is, by performing the double Fourier expansion

$$|\Psi(t)\rangle = \sum_{\{n_1,n_2\}=-\infty}^{\infty} |\psi_{n_1,n_2}(t)\rangle e^{in_1\omega_1 t}e^{in_2\omega_2 t}, \tag{21}$$

the Schrödinger equation leads to the set of coupled equations

$$\begin{aligned} i\hbar\frac{d|\psi_{n_1,n_2}\rangle}{dt} &= (H_0 + n_1\hbar\omega_1 + n_2\hbar\omega_2)|\psi_{n_1,n_2}\rangle \\ &\quad + \frac{1}{2}A_1X(|\psi_{n_1-1,n_2}\rangle + |\psi_{n_1+1,n_2}\rangle) + \frac{1}{2}A_2X \\ &\quad \times (e^{i\phi}|\psi_{n_1,n_2-1}\rangle + e^{-i\phi}|\psi_{n_1,n_2+1}\rangle). \end{aligned} \tag{22}$$

This is equivalent to a time-independent Schrödinger equation for the infinite state $|\Psi\rangle = \sum_{n_1,n_2}|\psi_{n_1,n_2}\rangle \otimes |n_1\rangle \otimes |n_2\rangle$ with the Floquet-Hamiltonian matrix

$$\begin{aligned} (\mathcal{H}_F)_{n,m} &= (H_0 + n_1\hbar\omega_1 + n_2\hbar\omega_2)\delta_{n,m} \\ &\quad + \tfrac{1}{2}A_1X(\delta_{n,m-e_1} + \delta_{n,m+e_1}) \\ &\quad + \tfrac{1}{2}A_2X(e^{i\phi}\delta_{n,m-e_2} + e^{-i\phi}\delta_{n,m+e_2}), \end{aligned} \tag{23}$$

where $n = \{n_1, n_2\}$, $m = \{m_1, m_2\}$, $e_1 = \{1, 0\}$, and $e_2 = \{0, 1\}$. To obtain the state amplitudes, one sums over the intermediate photon states

$$a_s(t) = \sum_{n_1,n_2} e^{i(n_1\omega_1 + n_2\omega_2)t}\langle s, n_1, n_2|\exp\left(-i\frac{\mathcal{H}_F t}{\hbar}\right)|\psi(0)\rangle, \tag{24}$$

where, in the following, we will assume that $|\psi(0)\rangle = |0, 0, 0\rangle$. The structure of these equations is well described elsewhere [29]. Here we make the following observations. First, to obtain accurate numerical results, one must include several photon states in the sum—including too few results in a loss of both accuracy and unitarity. Second, one can still use perturbation theory to obtain useful analytical results, provided one identifies the appropriate states of the combined system.

To illustrate this method we consider a particular example. Figure 1 shows the probability $p_1(t) = |a_1(t)|^2$ of the first excited state as a function of time for the system controlled by different control fields. The dashed curve is the result of a numerical simulation of the time-dependent Schrödinger equation for a phase qubit with $\omega_0/(2\pi) = 6$ GHz and $N_s = 4$ subject to a control field with $A_1 = 0.02\hbar\omega_0$ and $\omega_1 = \omega_{01}$. For this single-frequency pulse the maximum transition probability is approximately 90%. The solid curve is the result of a two-frequency control pulse with $A_2 = 0.0035\hbar\omega_0$, $\phi = 11.44$, $\omega_1 = \omega_{01} + \Omega_{01}^2/[2(\omega_{01} - \omega_{12})]$, and $\omega_2 = \omega_{12}$. The values of A_2 and ϕ were found by a numerical search to optimize the $0 \to 1$ transition. This pulse yields a maximum transition probability of nearly 99.9%, a significant improvement over the $A_2 = 0$ dynamics. This search was inspired by the general arguments given in Ref. [28] and demonstrates that the use of two frequencies can improve the control of this quantum system.

In addition to these time-dependent simulations, Fig. 1 also includes the result of a time-independent Floquet calculation performed by numerically diagonalizing $\mathcal{H}_F$ in a basis of 22 states, including up to three photons for each frequency. Here we provide an analytical approximation to explain this improved transition. Simulations suggest that a

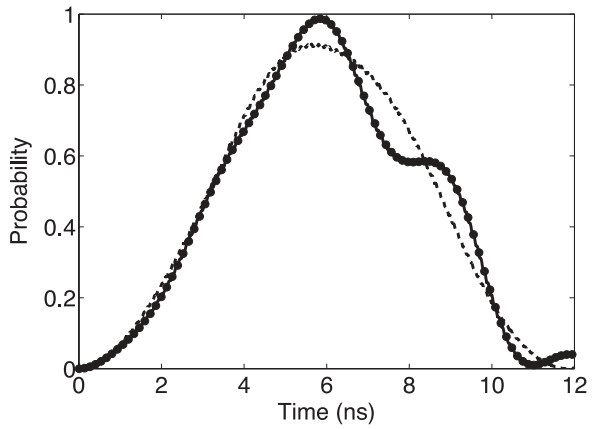

FIG. 1. Three-level Rabi oscillation. The probability $p_1(t) = |a_1(t)|^2$ to be in state 1 is shown as a function of time. The solid curve is a numerical simulation using an optimized control field with $A_1 = 0.02\hbar\omega_0$, $A_2 = 0.0035\hbar\omega_0$, and $\phi = 11.44$ rad, while the dots are calculations using the two-mode Floquet formalism. The dashed curve is a numerical simulation with $A_2 = 0$. Here, the system parameters were chosen to be $\omega_0/(2\pi) = 6$ GHz and $N_s = 4$. Other relevant parameters are $\Omega_1/(2\pi) = 86$ MHz, $\Omega_2/(2\pi) = 15$ MHz, $\omega_1/(2\pi) = 5.785$ GHz, $\omega_{01}/(2\pi) = 5.77$ GHz, and $\omega_2/(2\pi) = \omega_{12}/(2\pi) = 5.5$ GHz.

minimal model for this transition involves the states $|0, 0, 0\rangle$, $|1, -1, 0\rangle$, $|1, 0, -1\rangle$, $|2, -2, 0\rangle$, and $|2, -1, -1\rangle$. The Floquet Hamiltonian, in this basis, reads

$$\mathcal{H}_F = \hbar \begin{pmatrix} 0 & \Omega_1/2 & \Omega_2 e^{i\phi}/2 & 0 & 0 \\ \Omega_1/2 & -\delta & 0 & \Omega_1/\sqrt{2} & \Omega_2 e^{i\phi}/\sqrt{2} \\ \Omega_2 e^{-i\phi}/2 & 0 & \Delta & 0 & \Omega_1/\sqrt{2} \\ 0 & \Omega_1/\sqrt{2} & 0 & -\Delta_2 & 0 \\ 0 & \Omega_2 e^{-i\phi}/\sqrt{2} & \Omega_1/\sqrt{2} & 0 & -\delta \end{pmatrix}, \tag{25}$$

where $\hbar\Omega_1 = A_1 x_{01}$, $\hbar\Omega_2 = A_2 x_{01}$, $\delta = \omega_1 - \omega_{01}$, $\Delta = \omega_{01} - \omega_2$, $\Delta_2 = 2\omega_1 - \omega_{02}$, and we let $x_{12} = \sqrt{2}x_{01}$. By carefully normalizing and expanding out the terms found through perturbation theory we find

$$a_0(t) \approx \cos(\Omega_1 t/2)\left(1 - \frac{\Omega_2^2}{\Omega_1^2}[1 + \cos(2\phi)]\right) + 2\frac{\Omega_2^2}{\Omega_1^2}e^{i2\delta t}, \tag{26}$$

$$a_1(t) \approx -i\sin(\Omega_1 t/2)\left(1 - \frac{\Omega_1^2}{4\Delta^2} - \frac{\Omega_2^2}{\Omega_1^2}\cos(2\phi)\right) + \frac{\Omega_2}{2\Delta}e^{-i\phi}(1 + 2e^{i(\Delta+3\delta)t} - 3e^{i(\Delta+\delta)t}), \tag{27}$$

and

$$a_2(t) \approx -i\sin(\Omega_1 t/2)\frac{\sqrt{2}\Omega_1}{2\Delta}\left(1 - \frac{5\Omega_2}{2\Omega_1}e^{-i\phi}e^{i(\Delta+\delta)t}\right) - \cos(\Omega_1 t/2)\left(\frac{3\Omega_1^2}{4\sqrt{2}\Delta^2} - \frac{\sqrt{2}\Omega_2}{\Omega_1}e^{-i\phi}e^{i(\Delta+\delta)t}\right) - \frac{\sqrt{2}\Omega_2}{\Omega_1}e^{-i\phi}e^{i(\Delta+3\delta)t} + \frac{\Omega_1^2}{2\sqrt{2}\Delta}e^{i(\Delta+3\delta)t}. \tag{28}$$

We see that, in addition to the Rabi oscillation terms seen previously, there are terms that oscillate at the frequencies $\delta = \omega_1 - \omega_{01} = \Omega_1^2/(2\Delta)$ and $\Delta = \omega_{01} - \omega_{12}$. The former oscillations are slow and can typically be ignored, but the latter oscillations become important near the peaks of the Rabi oscillations. One can, in fact, use this to optimize the transition.

At time $T = \pi/\Omega_1$, many terms drop out of these amplitudes and by looking at the leading order terms of a_2, one finds that it will vanish provided

$$\Omega_2 e^{-i\phi} = \frac{\Omega_1^2}{2\Delta}e^{-i\pi/2}e^{-i(\Delta+3\delta)T}. \tag{29}$$

This condition, in turn, specifies the optimal amplitude and the phase of the second microwave drive. Thus, we identified a procedure to optimize the $0 \to 1$ transition by a controlled interference through the Floquet state dynamics. Using this value for ϕ and Ω_2, we find that the residual error scales as Ω_1^4/Δ^4, much better than the Ω_1^2/Δ^2 scaling found for a single-frequency transition.

V. NUMERICAL OPTIMIZATION

The analysis of the preceding section was motivated by optimizing numerically the amplitude and phase of the second frequency for the $0 \to 1$ transition. As shown, it was found that, by choosing the amplitude and phase appropriately, one can obtain significant improvement in the transition probability using control fields with constant amplitude, called square pulses. Here we compare the analytical results with the numerically optimized parameters and show how this approach can be used to generate optimized Gaussian pulses [11].

First, in Fig. 2, we show the numerically optimized $\Omega_2 = A_2 x_{01}/\hbar$ as a function of the bare Rabi frequency $\Omega_1 = A_1 x_{01}/\hbar$ for a phase qubit with $\omega_0/(2\pi) = 6$ GHz and $N_s = 4$, comparable to recent experiments [10]; other parameters can be found in Fig. 1. For this system, the anharmonicity is $\Delta/2\pi \approx 260$ MHz. We see that the analytical result

$$\Omega_{2,\mathrm{opt}} \approx \frac{\Omega_1^2}{2\Delta}, \tag{30}$$

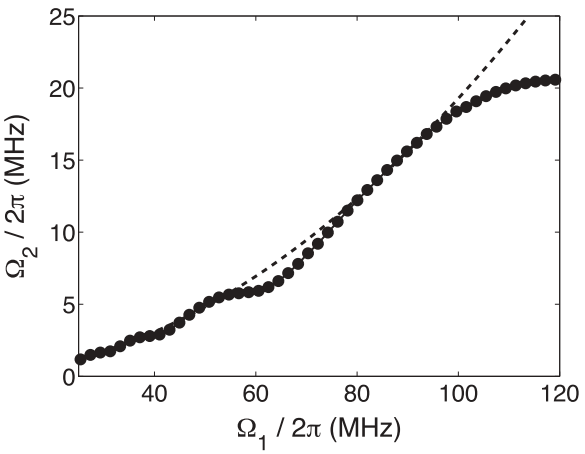

FIG. 2. Numerically optimized Ω_2 as a function of the primary Rabi frequency Ω_1. The dashed curve is the approximation $\Omega_2 \approx \Omega_1^2/(2\Delta)$ (see text).

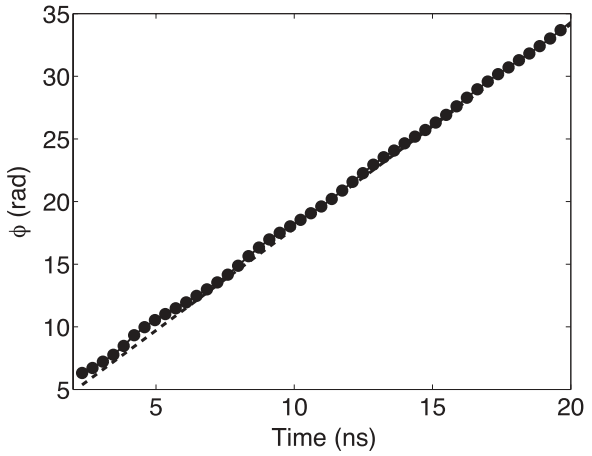

FIG. 3. Numerically optimized phase as a function of overall pulse time T. The dashed curve is the approximation $\phi \approx \pi/2 + \Delta T$ (see text).

provides an excellent approximation for the optimized amplitude. Similarly, the optimized phase ϕ is plotted as a function of the pulse time T in Fig. 3. As with the amplitude, the analytical result

$$\phi_{\text{opt}} \approx \frac{\pi}{2} + \Delta T, \tag{31}$$

provides an excellent approximation. As $\Delta = \omega_{01} - \omega_{12}$ is the difference in frequencies between the two transitions, we see that this value of ϕ ensures that the two transitions are combined with the appropriate phase at the final time.

As a further test of this method, we compare the error $p_E = 1 - p_1(T)$ for this two-frequency pulse with that of a single-frequency pulse. This is displayed in Fig. 4. The single-frequency pulse is seen to have an error that scales as Ω_1^2/Δ^2. The corresponding transition probability is between 90%–99%, improving only slowly for longer pulse times. The two-frequency pulse achieves a transition probability greater than 99.99% for pulses greater than 10 ns, a reduction of error by several orders of magnitude over the single-frequency pulse. The remaining error scales as $\Omega_1^4/16\Delta^4$, with oscillations of frequency Δ.

Finally, using this approach, one can design pulse shapes to further optimize the transition. We consider a Gaussian pulse shape

$$f(t) = s(t)\,[A_1 \cos(\omega_1 t) + A_2 \cos(\omega_2 t + \phi)], \tag{32}$$

with

$$s(t) = N_\alpha (e^{-\alpha(1-2t/T)^2} - e^{-\alpha}), \tag{33}$$

where α specifies the shape of the pulse and N_α is chosen such that $\int s(t)dt = T$ [11,16]. These pulses are optimized using the bare Rabi frequency

$$\Omega_1 = \frac{\pi}{T}\left(1 + c_\alpha \frac{\pi^2}{(\Delta T)^2}\right), \tag{34}$$

and drive frequency

$$\omega_1 = \omega_{01} + d_\alpha \frac{\pi^2}{\Delta T^2}, \tag{35}$$

where the dimensionless coefficients c_α and d_α are varied to obtain the best transition. These coefficients correct for the reduction in Rabi frequency and the ac Stark shift discussed previously and depend on the pulse shape parameter α. For $N_s = 4$ and $\alpha = 2$, we find that $c_{\alpha=2} = 0.58$ and $d_{\alpha=2} = 1.245$ are required. The error using Gaussian pulses with and without the Stark-shift correction is displayed in Fig. 5. We see that the single-frequency pulse is not effective without these corrections. To incorporate the two-frequency pulse, we numerically optimize for A_2 and ϕ and find that it provides a significant advantage. Note, however, that the two-frequency square pulse outperforms all of the Gaussian pulses for small pulse times.

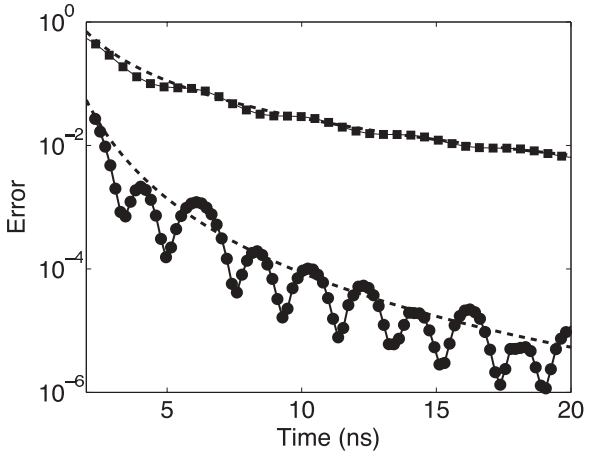

FIG. 4. Error of $0 \rightarrow 1$ transition using square pulses. The upper points (squares) are the error of a pulse using a single frequency with $\omega_1 = \omega_{01}$. The lower points (dots) are the error of an optimized two-frequency pulse with $\omega_1 = \omega_{01} + \Omega_1^2/(2\Delta)$ and $\omega_2 = \omega_{12}$. The upper dashed curve is $3\Omega^2/(4\Delta^2)$, while the lower dashed curve is $\Omega^4/(16\Delta^4)$ (see text).

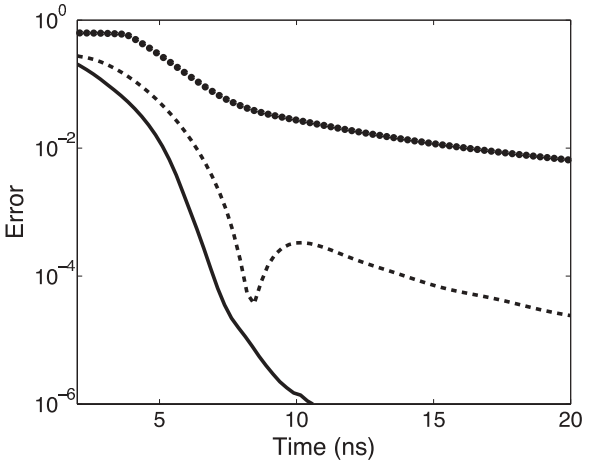

FIG. 5. Error of $0 \rightarrow 1$ transition using Gaussian pulses. The upper dotted curve is the error of a pulse using a single frequency with $\omega_1 = \omega_{01}$. The dashed curve is the error of a single-frequency pulse with $\omega_1 = \omega_{01} + d_2\Omega_1^2/(2\Delta)$. The lower solid curve is the error of an optimized two-frequency pulse with $\omega_2 = \omega_{12}$ (see text).

VI. THREE-STATE OSCILLATIONS

Recently, multifrequency control of multiple levels of a superconducting circuit was experimentally demonstrated [10]. This phase qudit was used to emulate spin-1 and spin-3/2 quantum systems. Here we look at the spin-1 case and show how the two-mode Floquet theory explains the nature of the three-state oscillations at high microwave power.

Figure 6 shows the state-2 probability $p_2(t)$, when the control field is chosen with $A_1 = 0.01\hbar\omega_0$, $\omega_1 = \omega_{01}$, $\omega_2 = \omega_{12}$ and $\hbar\Omega = A_1 x_{01} = A_2 x_{12}$. Using the rotating-wave approximation, one expects the dynamics to emulate the rotation of a spin-1 system, yielding a probability to be in state 2 of

$$p_2(t) = \sin^4\left(\frac{\Omega t}{2\sqrt{2}}\right). \tag{36}$$

While it is expected that there may be Stark shifts, corrections to the Rabi frequencies, and off-resonant transitions for this square pulse a qualitatively new effect is seen in the numerical simulation. This is a beating at the frequency $\Delta = \omega_1 - \omega_2$.

Using the Floquet formalism, one finds that the dominant effect is a coupling between three photon blocks of the three-level system or a total of nine states: $|0,-1,1\rangle$, $|1,-2,1\rangle$, $|2,-2,0\rangle$, $|0,0,0\rangle$, $|1,-1,0\rangle$, $|2,-1,-1\rangle$, $|0,1,-1\rangle$, $|1,0,-1\rangle$, and $|2,0,-2\rangle$. In this basis the effective Hamiltonian is

$$\mathcal{H}_F = \hbar \begin{pmatrix}
-\Delta & \Omega/2 & 0 & 0 & \frac{1}{2}\Omega/\sqrt{2} & 0 & 0 & 0 & 0 \\
\Omega/2 & -\Delta & \Omega/2 & 0 & 0 & 0 & 0 & 0 & 0 \\
0 & \Omega/2 & -\Delta & 0 & \Omega/\sqrt{2} & 0 & 0 & 0 & 0 \\
0 & 0 & 0 & 0 & \Omega/2 & 0 & 0 & \frac{1}{2}\Omega/\sqrt{2} & 0 \\
\frac{1}{2}\Omega/\sqrt{2} & 0 & \Omega/\sqrt{2} & \Omega/2 & 0 & \Omega/2 & 0 & 0 & 0 \\
0 & 0 & 0 & 0 & \Omega/2 & 0 & 0 & \Omega/\sqrt{2} & 0 \\
0 & 0 & 0 & 0 & 0 & 0 & \Delta & \Omega/2 & 0 \\
0 & 0 & 0 & \frac{1}{2}\Omega/\sqrt{2} & 0 & \Omega/\sqrt{2} & \Omega/2 & \Delta & \Omega/2 \\
0 & 0 & 0 & 0 & 0 & 0 & 0 & \Omega/2 & \Delta
\end{pmatrix}. \tag{37}$$

Note that one three-level block is isomorphic to a spin operator for a spin-1 system.

By performing the lowest order of perturbation theory for the coupling between blocks of $\mathcal{H}_F$, one finds that the relevant transition amplitude is

$$a_2(t) \approx -\sin^2\left(\frac{\Omega t}{2\sqrt{2}}\right) - i\frac{\Omega}{4\Delta}\sin\left(\frac{\Omega t}{\sqrt{2}}\right)(1 + 2e^{-i\Delta t}). \tag{38}$$

This provides an excellent approximation to the beating observed in Fig. 6. Note that the perturbation, which is proportional to Ω/Δ, happens to vanish precisely when the unperturbed oscillation reaches its maximum ($t = \sqrt{2}\pi/\Omega$). Thus, it is likely that additional effects limit this approach to a $0 \to 2$ transition. By extending the matrix to 15 states and higher orders in perturbation theory, one finds a state-3 population proportional to Ω^2/Δ^2.

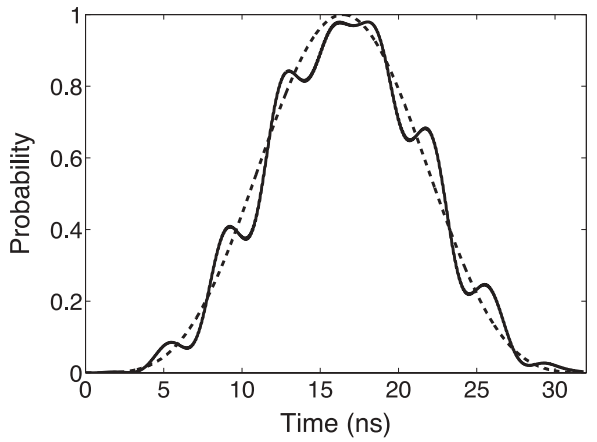

FIG. 6. Effective spin rotation from $0 \to 2$. The probability $p_2(t)$ to be in state 2 is shown as a function of time. The solid curve is a numerical simulation using $A_1 = 0.01\hbar\omega_0$ and $A_2 = A_1 x_{01}/x_{12}$ with parameters of Fig. 1. The dashed curve is the expected rotation obtained by using the rotating-wave approximation.

VII. CONCLUSION

In this article we analyze a set of multilevel effects found in superconducting circuits such as the phase or transmon qubit when controlled by pulses with two microwave frequencies. These involve a combination of resonant, off-resonant, and interference effects that are of importance for future qubit (or qudit) superconducting implementations of quantum information processors. Indeed, we demonstrate that the many-mode Floquet formalism for multiple frequencies is a useful generalization of the standard rotating-wave approximation.

First, we use the single-mode formalism to recover compact analytical results for corrections to Rabi oscillations in a three-level system, finding corrections to both the resonance condition and the oscillation frequency of relative order Ω^2/Δ^2.

These are the ac Stark shift and reduction in Rabi frequency seen in existing experiments and predicted previously.

Second, we show that simultaneously controlling the qubit with two frequencies, one resonant with the $0 \rightarrow 1$ transition (after compensating for the ac Stark shift) and the other resonant with the $1 \rightarrow 2$ transition, leads to a useful interference effect. This insight was inspired by numerical results on square pulses and found to be in excellent agreement. This approach was further extended numerically to show that two-frequency Gaussian pulses can be developed for the $0 \rightarrow 1$ transition with significant improvements over single-frequency pulses.

Finally, we use the Floquet method to explain off-resonant couplings that emerge when using the phase qudit to emulate a spin system. Here we find and explain a beating that is proportional to Ω/Δ and should be observable in recent experiments, provided it is not masked by the effects of decoherence.

For these effects to be genuinely useful, one would like to extend the optimization of a transition between two (or more) states to the optimization of a unitary operation acting an a superposition of these states. Here, however, an interesting difficulty emerges. For the single-frequency pulse with square or Gaussian shapes this is immediate: This control pulse is symmetric under time reversal: $f(-t) = f(t)$. Consequently, the transition from $0 \rightarrow 1$ and its time reverse from $1 \rightarrow 0$ are both optimized for a single $f(t)$. For the two-frequency pulse, however, $f(-t) \neq f(t)$, and in fact, the optimization developed in Sec. III does not perform as well for the $1 \rightarrow 0$ transition. Note that this observation sheds some light on the two-quadrature approach of Ref. [16]: The class of control pulses advocated there is time-reversal symmetric. We expect that combining multiple quadratures and multiple frequencies will significantly expand the control techniques for future experiments. Developing simple, accurate control pulses for multilevel quantum systems remains a challenging problem for theory and experiment.

APPENDIX

In this Appendix we summarize the perturbative results for the cubic oscillator

$$H = \hbar\omega_0\left(\tfrac{1}{2}p^2 + \tfrac{1}{2}x^2 - \lambda x^3\right). \tag{A1}$$

We use Rayleigh-Schrödinger perturbation theory for the Hamiltonian $H = H_0 + \lambda V$. First, one expresses the nth energy eigenstate, $|\Psi_n\rangle$, in powers of λ

$$|\Psi_n\rangle = \sum_{k=0}^{\infty} \lambda^k |n,k\rangle. \tag{A2}$$

In this expansion, $|n,0\rangle = |n\rangle$ is the nth energy eigenstate of H_0 and $|n,k\rangle$ are the kth order perturbative corrections. We also expand the energy eigenvalue in powers of λ,

$$E_n = \sum_{k=0}^{\infty} \lambda^k E_{n,k}, \tag{A3}$$

where $H_0|n,0\rangle = E_{n,0}|n,0\rangle$. Substituting (A2) and (A3) in the eigenvalue equation

$$(H_0 + \lambda V)|\Psi_n\rangle = E_n|\Psi_n\rangle, \tag{A4}$$

equating like powers of λ^k and projecting onto $\langle m,0|$ allows one to solve for the energies and eigenfunctions:

$$E_{n,k} = \langle n,0|V|n,k-1\rangle, \tag{A5}$$

and

$$|n,k\rangle = \sum_{m\neq n} \frac{\langle m,0|V|n,k-1\rangle - \sum_{j=1}^{k-1} E_{n,j}\langle m,0|n,k-j\rangle}{E_{n,0} - E_{m,0}} \times |m,0\rangle. \tag{A6}$$

These results for the eigenstates and eigenvalues can be evaluated using the matrix elements of x^3, where $x = (a + a^\dagger)/\sqrt{2}$ is the dimensionless position operator in terms of creation and annihilation operators. Extending this calculation for the energy to λ^8 one finds

$$\begin{aligned} E_n/\hbar\omega_0 = {} & (n+1/2) - \frac{1}{8}\lambda^2(30n^2+30n+11) \\ & - \frac{15}{32}\lambda^4(94n^3+141n^2+109n+31) \\ & - \frac{1}{128}\lambda^6(115755n^4+231510n^3+278160n^2 \\ & + 162405n + 39709) - \frac{21}{2048}\lambda^8(2282682n^5 \\ & + 5706706n^4 + 9387690n^3 + 8374830n^2 \\ & + 4244573n + 916705). \end{aligned} \tag{A7}$$

This procedure was implemented in MATHEMATICA to calculate the eigenvalues up to λ^6; the λ^8 in expression (A7) was found using a more efficient recursion-relation method [33] and agrees with Ref. [34] (provided one lets $4^N \rightarrow 4^{2N}$). These results, when compared with numerical results found by complex scaling [35], are found to have an accuracy better than 1% for states $n = 0 \rightarrow 2$ when $N_s > 3$.

In addition to the energy levels, perturbation theory also provides expressions for the wave functions. For reference, we list the third-order expression

$$\begin{aligned} |\Psi_n\rangle = {} & |n\rangle + \lambda \sum_{k=-3}^{+3} a_k(n)|n+k\rangle + \lambda^2 \sum_{k=-6}^{+6} b_k(n)|n+k\rangle \\ & + \lambda^3 \sum_{k=-9}^{+9} c_k(n)|n+k\rangle, \end{aligned} \tag{A8}$$

where $|n\rangle = |n,0\rangle$ are the eigenstates of the purely harmonic oscillator Hamiltonian and the nonzero expansion coefficients are

$$a_{-3}(n) = -\frac{1}{6\sqrt{2}}\left[n(n-1)(n-2)\right]^{1/2}, \tag{A9}$$

$$a_{-1}(n) = -\frac{3}{2\sqrt{2}}n^{3/2}, \tag{A10}$$

$$a_{+1}(n) = -\frac{3}{2\sqrt{2}}(n+1)^{3/2}, \tag{A11}$$

$$a_{+3}(n) = \frac{1}{6\sqrt{2}}\left[(n+1)(n+2)(n+3)\right]^{1/2}, \tag{A12}$$

$$b_{-6}(n) = \frac{1}{144}\left[n(n-1)(n-2)(n-3)(n-4)(n-5)\right]^{1/2}, \tag{A13}$$

$$b_{-4}(n) = \frac{1}{32}\,[n(n-1)(n-2)(n-3)]^{1/2}\,(4n-3), \quad \text{(A14)}$$

$$b_{-2}(n) = \frac{1}{16}\,[n(n-1)]^{1/2}\,(7n^2-19n+1), \quad \text{(A15)}$$

$$b_{+2}(n) = \frac{1}{16}\,[(n+1)(n+2)]^{1/2}\,(7n^2+33n+27), \quad \text{(A16)}$$

$$b_{+4}(n) = \frac{1}{32}\,[(n+1)(n+2)(n+3)(n+4)]^{1/2}\,(4n+7), \quad \text{(A17)}$$

$$b_{+6}(n) = \frac{1}{144}[(n+1)(n+2)(n+3) \times (n+4)(n+5)(n+6)]^{1/2}, \quad \text{(A18)}$$

and

$$c_{-9}(n) = -\frac{1}{2592\sqrt{2}}[n(n-1)(n-2)(n-3)(n-4) \times (n-5)(n-6)(n-7)(n-8)],^{1/2} \quad \text{(A19)}$$

$$c_{-7}(n) = -\frac{1}{192\sqrt{2}}[n(n-1)(n-2)(n-3)(n-4) \times (n-5)(n-6)]^{1/2}(2n-3), \quad \text{(A20)}$$

$$c_{-5}(n) = -\frac{1}{960\sqrt{2}}[n(n-1)(n-2)(n-3) \times (n-4)]^{1/2}(80n^2-305n+164), \quad \text{(A21)}$$

$$c_{-3}(n) = -\frac{1}{1728\sqrt{2}}[n(n-1)(n-2)]^{1/2}(488n^3 - 2175n^2+4018n-825), \quad \text{(A22)}$$

$$c_{-1}(n) = -\frac{3}{64\sqrt{2}}n^{1/2}(20n^4+81n^3+326n^2+81n+44), \quad \text{(A23)}$$

$$c_{+1}(n) = \frac{3}{64\sqrt{2}}(n+1)^{1/2}(20n^4-n^3 + 203n^2+408n+228), \quad \text{(A24)}$$

$$c_{+3}(n) = \frac{1}{1728\sqrt{2}}[(n+1)(n+2)(n+3)]^{1/2}(488n^3 + 3639n^2+9832n+7506), \quad \text{(A25)}$$

$$c_{+5}(n) = \frac{1}{960\sqrt{2}}[(n+1)(n+2)(n+3)(n+4) \times (n+5)]^{1/2}(80n^2+465n+549), \quad \text{(A26)}$$

$$c_{+7}(n) = \frac{1}{192\sqrt{2}}[(n+1)(n+2)(n+3)(n+4) \times (n+5)(n+6)(n+7)]^{1/2}(2n+5), \quad \text{(A27)}$$

$$c_{+9}(n) = \frac{1}{2592\sqrt{2}}[(n+1)(n+2)(n+3)(n+4)(n+5) \times (n+6)(n+7)(n+8)(n+9)]^{1/2}. \quad \text{(A28)}$$

One application of these expressions is to calculate the (properly normalized) matrix elements of the position operator

$$x_{n,m} = \frac{\langle\Psi_n|x|\Psi_m\rangle}{(\langle\Psi_n|\Psi_n\rangle\langle\Psi_m|\Psi_m\rangle)^{1/2}}. \quad \text{(A29)}$$

Using the wave functions (A8) and matrix elements of x, we find

$$x_{0,0} = \frac{3}{2}\lambda + \frac{33}{2}\lambda^3, \quad \text{(A30)}$$

$$x_{0,1} = \frac{\sqrt{2}}{2} + \frac{11\sqrt{2}}{8}\lambda^2, \quad \text{(A31)}$$

$$x_{0,2} = -\frac{\sqrt{2}}{2}\lambda - \frac{243\sqrt{2}}{16}\lambda^3, \quad \text{(A32)}$$

$$x_{0,3} = \frac{3\sqrt{3}}{8}\lambda^2, \quad \text{(A33)}$$

$$x_{1,1} = \frac{9}{2}\lambda + \frac{213}{2}\lambda^3, \quad \text{(A34)}$$

$$x_{1,2} = 1 + \frac{11}{2}\lambda^2, \quad \text{(A35)}$$

$$x_{1,3} = -\frac{\sqrt{6}}{2}\lambda - \frac{405\sqrt{6}}{16}\lambda^3, \quad \text{(A36)}$$

$$x_{2,2} = \frac{15}{2}\lambda + \frac{573}{2}\lambda^3, \quad \text{(A37)}$$

$$x_{2,3} = \frac{\sqrt{6}}{2} + \frac{33\sqrt{6}}{8}\lambda^2, \quad \text{(A38)}$$

$$x_{3,3} = \frac{21}{2}\lambda + \frac{1113}{2}\lambda^3, \quad \text{(A39)}$$

with corrections of order λ^4.

[1] J. M. Martinis, S. Nam, J. Aumentado, and C. Urbina, Phys. Rev. Lett. **89**, 117901 (2002).

[2] J. M. Martinis *et al.*, Phys. Rev. Lett. **95**, 210503 (2005).

[3] I. Siddiqi, R. Vijay, M. Metcalfe, E. Boaknin, L. Frunzio, R. J. Schoelkopf, and M. H. Devoret, Phys. Rev. B **73**, 054510 (2006).

[4] F. Yoshihara, K. Harrabi, A. O. Niskanen, Y. Nakamura, and J. S. Tsai, Phys. Rev. Lett. **97**, 167001 (2006).

[5] J. A. Schreier *et al.*, Phys. Rev. B **77**, 180502(R) (2008).

[6] A. A. Houck *et al.*, Phys. Rev. Lett. **101**, 080502 (2008).

[7] R. Fazio, G. M. Palma, and J. Siewert, Phys. Rev. Lett. **83**, 5385 (1999).

[8] F. W. Strauch, P. R. Johnson, A. J. Dragt, C. J. Lobb, J. R. Anderson, and F. C. Wellstood, Phys. Rev. Lett. **91**, 167005 (2003).

[9] G. K. Brennen, D. P. O'Leary, and S. S. Bullock, Phys. Rev. A **71**, 052318 (2005).

[10] M. Neeley *et al.*, Science **325**, 722 (2009).

[11] M. Steffen, J. M. Martinis, and I. L. Chuang, Phys. Rev. B **68**, 224518 (2003).

[12] M. H. S. Amin, Low Temp. Phys. **32**, 198 (2006).

[13] P. Rebentrost and F. K. Wilhelm, Phys. Rev. B **79**, 060507(R) (2009).

[14] S. Safaei, S. Montangero, F. Taddei, and R. Fazio, Phys. Rev. B **79**, 064524 (2009).

[15] H. Jirari, F. W. J. Hekking, and O. Buisson, Europhys. Lett. **87**, 28004 (2009).

[16] F. Motzoi, J. M. Gambetta, P. Rebentrost, and F. K. Wilhelm, Phys. Rev. Lett. **103**, 110501 (2009).

[17] P. R. Johnson, F. W. Strauch, A. J. Dragt, R. C. Ramos, C. J. Lobb, J. R. Anderson, and F. C. Wellstood, Phys. Rev. B **67**, 020509(R) (2003).
[18] J. Koch, T. M. Yu, J. Gambetta, A. A. Houck, D. I. Schuster, J. Majer, A. Blais, M. H. Devoret, S. M. Girvin, and R. J. Schoelkopf, Phys. Rev. A **76**, 042319 (2007).
[19] J. M. Chow, J. M. Gambetta, L. Tornberg, J. Koch, L. S. Bishop, A. A. Houck, B. R. Johnson, L. Frunzio, S. M. Girvin, and R. J. Schoelkopf, Phys. Rev. Lett. **102**, 090502 (2009).
[20] L. DiCarlo *et al.*, Nature **460**, 240 (2009).
[21] J. Claudon, F. Balestro, F. W. J. Hekking, and O. Buisson, Phys. Rev. Lett. **93**, 187003 (2004).
[22] J. Claudon, A. Zazunov, F. W. J. Hekking, and O. Buisson, Phys. Rev. B **78**, 184503 (2008).
[23] S. K. Dutta *et al.*, Phys. Rev. B **78**, 104510 (2008).
[24] E. Lucero, M. Hofheinz, M. Ansmann, R. C. Bialczak, N. Katz, M. Neeley, A. D. O'Connell, H. Wang, A. N. Cleland, and J. M. Martinis, Phys. Rev. Lett. **100**, 247001 (2008).
[25] M. A. Sillanpää, J. Li, K. Cicak, F. Altomare, J. I. Park, R. W. Simmonds, G. S. Paraoanu, and P. J. Hakonen, Phys. Rev. Lett. **103**, 193601 (2009).
[26] K. V. R. M. Murali, Z. Dutton, W. D. Oliver, D. S. Crankshaw, and T. P. Orlando, Phys. Rev. Lett. **93**, 087003 (2004).
[27] Z. Dutton, K. V. R. M. Murali, W. D. Oliver, and T. P. Orlando, Phys. Rev. B **73**, 104516 (2006).
[28] L. Tian and S. Lloyd, Phys. Rev. A **62**, 050301(R) (2000).
[29] T. S. Ho, S. I. Chu, and J. V. Tietz, Chem. Phys. Lett. **96**, 464 (1983).
[30] J. H. Shirley, Phys. Rev. **138**, B979 (1965).
[31] F. Meier and D. Loss, Phys. Rev. B **71**, 094519 (2005).
[32] F. W. Strauch *et al.*, IEEE Trans. Appl. Supercond. **17**, 105 (2007).
[33] C. M. Bender and G. V. Dunne, J. Math. Phys. **40**, 4616 (1999).
[34] G. Alvarez, J. Phys. A **22**, 617 (1989).
[35] R. Yaris, J. Bendler, R. A. Lovett, C. M. Bender, and P. A. Fedders, Phys. Rev. A **18**, 1816 (1978).